A non-invasive approach to awake mouse fMRI compatible with multi-modal techniques

Sam Laxer[1,2], Amr Eed[1], Miranda Bellyou[1], Peter Zeman[1], Kyle M Gilbert[1,2], Mohammad Naderi[1], Ravi S Menon[1,2]

[1]Centre for Functional and Metabolic Mapping, Western University, London, Ontario, Canada
[2]Department of Medical Biophysics, Western University, London, Ontario, Canada

Abstract

Mouse functional magnetic resonance imaging (fMRI) studies contribute significantly to neuroimaging research, playing an important role in advancing our understanding of the human brain. Efforts to scan mice in the awake state and avoid the use of anesthesia have demonstrated many benefits. However, the majority of current awake fMRI approaches involve head fixation through invasive surgical means. These approaches are limited for several reasons including increased subject morbidity and mortality, prolonged study timelines due to surgical recovery, a higher risk of susceptibility artifacts contaminating T2*-weighted images and obstructed access to the head for multi-modal recording techniques such as electrophysiology and fibre photometry. To address this need, we propose a non-invasive restraint to scan mice in the awake state. The restraint was designed to be compatible with brain stimulation and recording approaches. It was evaluated on the basis of motion, fMRI data quality, and animal stress levels, and subsequently compared to a conventional headpost restraint. We found the proposed approach was effective at restraining mice across a broad range of weights without the need for any anesthesia for setup. Conservatively, acquiring 25% more data with the non-invasive restraint compensates for censored frames in high motion runs and results in comparable network spatial specificity to less motion-vulnerable headpost approaches. This validation of network robustness paired with its non-invasive nature makes it a favourable approach for applications requiring high-throughput and/or multimodal imaging studies.

1 Introduction

Functional magnetic resonance imaging (fMRI) is an important tool in neuroscience for characterizing brain-wide networks in healthy animals and disease models. Mice have been particularly beneficial due to the wide range of available transgenic lines and the high translational value due to their similar neurophysiology compared to humans (Mandino et al., 2020, 2021; N. Xu et al., 2022) . However, motion needs to be minimized to acquire useful data (Power et al., 2012). To control motion, there are currently 3 main scanning approaches: 1) using anesthesia, 2) scanning awake using an invasive restraint, and 3) scanning awake using a non-invasive restraint.

Anesthesia in mice has been common practice in fMRI research due to its effectiveness, however an increasing number of studies have shown its confounding effects on brain hemodynamics and networks (Dinh et al., 2021; Gao et al., 2017; Gutierrez-Barragan et al., 2022). These include damped and lagged hemodynamic responses compared to the unanesthetized brain and altered functional connectivity. Therefore, when the research goal is understanding physiology or maintaining a high translational value, scanning mice in an awake state provides considerable advantages.

This motivated the development of awake invasive approaches, often utilizing surgically implanted headposts as a fixation point on the skull (Chen et al., 2020; Gutierrez-Barragan et al., 2022). This approach avoids the negative effects of anesthesia (after the initial surgery) and in some cases allows for comparable motion control to anesthesia. Despite these benefits, the use of a headpost poses challenges in many applications. These include: 1) the headpost obstructing access to the skull when simultaneous multimodal recording is desired (such as combining fMRI with fibre photometry, optogenetics, or electrophysiology), 2) vulnerable or highly valuable mouse lines being unable or posing too great of a risk to undergo headpost implantation surgery (Szilagyi et al., 2018; Wu et al., 2020), 3) the headposts, cement or associated surgical procedures causing MRI distortion artifacts, or 4) having high-throughput studies with a very large number of subjects makes surgical approaches impractical. One solution is to develop non-invasive awake imaging approaches that forego the use of a headpost while maintaining awake imaging.

Non-invasive restraints have been developed in the past (Fadel et al., 2022; Ferris, 2022; Harris et al., 2015; Madularu et al., 2017) and are quite common for rat studies. However, the current mouse systems suffer from tedious animal setup procedures often requiring the brief administration of anesthesia to position the mice and some holders are not compatible with the small inner diameter size of high-performance gradient inserts. The success of rat systems is due to the larger size of the animal and their better ability to be trained compared to mice (Ellenbroek & Youn, 2016; Parker et al., 2014). Thus, there remains a need for a simple, effective non-invasive restraint ideally requiring no anesthesia for animal setup.

Another barrier concerning awake imaging approaches is stress. Animal stress has been investigated and shown to impact hemodynamics and results in stress-related motion, while also imposing a negative impact on the animal's wellbeing (Low et al., 2016). Consequently, a large effort has been made to develop restraint features and associated procedures to minimize stress. To this end, various labs have developed acclimation procedures to gradually expose subjects to restraint and the scanning environment (i.e., dark and loud environment mimicking the auditory and visual experience of the scanner) (Chen et al., 2020; Desjardins et al., 2019; Dinh et al., 2021; Gutierrez-Barragan et al., 2022; Takata et al., 2018). Additionally, care has been taken to design restraints such that subject comfort is improved to further reduce stress (W. Xu et al., 2022).

Here, we present an approach to non-invasive awake-mouse MRI with a focus on compatibility with multi-modal experiments – all while remaining small enough to fit inside the 60-mm-diameter gradient coil found in many small bore animal MRI scanners. The developed restraint allows for effective motion control and no need for anesthesia during animal setup. Motion and dual-regression-based resting state network robustness were evaluated in comparison with a typical headpost restraint approach. Lastly, stress was analyzed by measuring weight and corticosterone changes between three different acclimation procedures in both sexes.

2 Methods

2.1 Ethics Statement

All experimental methods described were performed in accordance with the guidelines of the Canadian Council on Animal Care policy on the care and use of experimental animals and an ethics protocol approved by the Animal Care Committee of The University of Western Ontario.

2.2 Subjects and Groups

This study involved 40 wildtype C57BL/6 mice from Jackson Laboratories (n = 13) and Charles River Laboratories (n = 28). Mice were divided into 4 groups (Table 1) with each group having roughly equally proportions of males and females. Groups 1, 2 and 3 underwent the non-invasive imaging protocol (with differing acclimation lengths) and Group 4 underwent a conventional headpost imaging protocol with the same acclimation protocol as the non-invasive 9-day protocol as shown in Table 2. Animals in Groups 1, 2, and 3 were single-housed in a facility with a 12-hour light/dark cycle (light from 7:00 am – 7:00 pm) and fed food and water ad-libitum. Animals were single-housed to replicate the treatment for cannula-implanted mice who are single-housed to minimize the risk of mouse cage mates damaging/removing each other's cannulas. Mice in Group 4 (acquired previously) were group-housed.

Table 1. Subject information. The first 4 rows display the sample sizes in each group (m = males, f = females).

Parameter	Value
Group 1 (Non-invasive – 4-day protocol)	4 m + 5 f
Group 2 (Non-invasive – 9-day protocol)	4 m + 5 f
Group 3 (Non-invasive – 13-day protocol)	7 m + 8 f
Group 4 (Headpost – 9-day protocol)	4 m + 3 f
Strain	C57BL/6
Age range	2 – 35 weeks
Weight range	16 – 37 g

2.3 Restraint designs

The non-invasive restraint is almost entirely 3D printed of polycarbonate (Figure *1*). It consists of a cylindrical body tube, a neck plate to keep the subject in position, and the combination of a bite bar and two head arches (one anterior at the snout and one posterior at the caudal end of the skull) to stabilize the head in all three dimensions. An in-house built single-loop transmit/receive coil was designed to fit over top of the head after the arches were secured.

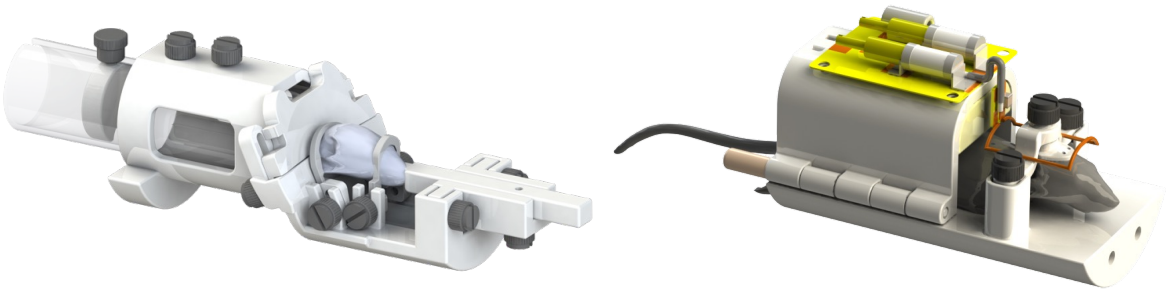

Figure 1. CAD models of the non-invasive restraint (left) and headpost restraint (right). The single loop coil used for single transmit/receive is not shown on the non-invasive restraint to allow clear visualization of the arches over the mouse head.

The headpost-style restraint is also 3D printed using polycarbonate. It was initially inspired by a headpost designed by (Gutierrez-Barragan et al., 2022), with further modifications. Rather than permanently implanting the large 'head-bar wing', we implanted a small threaded collar on the skull to allow for the attachment of the 'head-bar wing' when the mouse is to be restrained. The motivation was to provide less of an impediment to the natural movement of a mouse in their cage when unrestrained.

All designs have been made freely available (https://doi.org/10.17605/OSF.IO/TYHCE).

2.4 Surgery

Mice in group 4 underwent surgery to have headposts implanted on their skulls. Mice were initially anesthetized with 4% isoflurane in oxygen and then switched to a 1.7 – 2 % mixture for maintenance. Once deeply anesthetized (confirmed using toe pinch), mice were injected with 0.05 mL/kg of Meloxicam to reduce postoperative pain and 0.05 mL/kg of Lidocaine to numb the surgical area. The hair on the scalp was removed with an electronic razor, eye ointment was applied, and a rectal thermometer was used to record temperature throughout the surgery. The mouse was placed in a stereotactic frame (71000 Automated Stereotaxic Instrument, RWD Life Science) and positioned with the skull level. After sterilizing the scalp, the skin above the skull was removed, and the soft tissue was cleared away. The skull was cleaned with saline and dried. The skull was then lightly scraped to provide a better surface for the bonding agent to adhere to. The bonding agent (All-Bond Universal, Bisco Dental) was applied to the skull and cured using an ultraviolet light. Dental cement (CoreFlo DC Lite, Bisco Dental) was subsequently applied, and the headpost was pressed onto the skull maintaining a high, constant pressure. The dental cement was cured, then the remaining exposed skull was covered with dental cement and cured. The mouse was then released from the stereotactic device and began a 10-day period of recovery prior to restraint acclimation. Additional injections of Meloxicam were given 24 and 48 hours after surgery.

2.5 Acclimation protocols

Three different acclimation protocols were used in the present study. Short (4-day; Group 1), medium (9-day; Groups 2 and 4) and long (13-day; Group 3) protocols were devised. The details for each protocol are shown in Table 2. These were designed to represent protocols typically used in recent literature (refer to (Mandino et al., 2023)).

Table 2. Protocol used to acclimate each Group. Group 1 underwent the 4-day protocol (left), Group 2 and the headpost group underwent the 9-day protocol (middle) and Group 3 underwent the 13-day protocol (right).

Day	Duration	Procedure
1	15 min	Manual handling (0 dB)
2	30 min	Restrained (0 dB)
3	45 min	Restrained (75 dB)
4	1 hr	Restrained (100 dB)

Day	Duration	Procedure
1	15 min	Manual handling (0 dB)
2	10 min	Restrained (0 dB)
3	20 min	Restrained (0 dB)
4	30 min	Restrained (50 dB)
5	45 min	Restrained (75 dB)
6	1 hr	Restrained (100 dB)
7	1 hr 15 min	Restrained (100 dB)
8	1 hr 30 min	Restrained (100 dB)
9	1 hr 30 min	Restrained (100 dB)

Day	Duration	Procedure
1	15 min	Manual handling (0 dB)
2	10 min	Restrained (0 dB)
3	15 min	Restrained (0 dB)
4	20 min	Restrained (50 dB)
5	30 min	Restrained (75 dB)
6	45 min	Restrained (75 dB)
7	45 min	Restrained (75 dB)
8	1 hr	Restrained (75 dB)
9	1 hr	Restrained (75 dB)
10	1 hr 15 min	Restrained (100 dB)
11	1 hr 30 min	Restrained (100 dB)
12	1 hr 30 min	Restrained (100 dB)
13	1 hr 30 min	Restrained (100 dB)

All acclimation sessions were started at approximately the same time each day to account for differences in circadian rhythm. Day 1 consisted of the same procedure for Groups 1, 2, and 3. Specifically, mice were introduced to the restraint and allowed to freely explore it for the first few minutes. For the remaining duration of the session, mice would be encouraged to walk through the restraint. This involved the researcher picking up the mouse by the tail and guiding the subject into the apparatus. After successfully walking through the tube, a chocolate sprinkle would be provided as a reward. Subsequently, the subject would be repeatedly encouraged to walk through the restraint to establish that movement. Importantly, day 1 does not involve restraint. Each of the following sessions starts with this exercise for the first few minutes to encourage the intended behaviour.

Restraining the mouse using the proposed non-invasive restraint involves 3 steps: 1) broad restraint, 2) bite bar, and 3) fine restraint. Step 1 consists of letting the mouse walk through the body tube as performed previously but stopping the subject after their head passes through the neck plate and carefully lowering the neck plate into position. This effectively prevents the subject from moving further forward or backward in the restraint. To gradually expose mice to being fully restrained, Day 2 of each session consists of keeping the mouse in this coarsely restrained position only. Day 3 of training onwards involves all 3 restraint steps. Step 2 of restraint uses the bite bar and anterior arch. This involves using the anterior arch to control the subject's snout and guide the top front teeth (incisors) into the bite bar groove. Once in position, the bite bar and anterior arch are secured in place with fastening screws. Finally, step 3 is implemented consisting of the posterior arch being positioned over the posterior aspect

of the subject's head. Effectively, the neckplate and body tube prevent broad motion, and the combination of the bite bar, anterior arch and posterior arch prevent fine motion.

2.6 Mock scanner

It is common practice to design a "mock scanner" to simulate the scanning experience (Dinh et al., 2021; Lindhardt et al., 2022). This has the added benefit of allowing for a more gradual acclimation as subjects can be exposed to restraint and MRI sounds independently. The mock scanner apparatus consists of a large box (65 cm wide, 52 cm long and 44 cm high) with PVC pipes placed inside allowing for multiple animals to be acclimated simultaneously. A Bluetooth speaker is also placed in the box to play MRI sounds at designated sound levels (Table 2). The mock sounds were selected as the same sequences used to scan the subjects during acquisition. The audio was recorded using a fibre optic microphone (OptiSLM, OptoAcoustics Ltd) placed next to the magnet. Both the gradient-echo echo planar imaging (GE-EPI) sequence and anatomical Turbo RARE sequence were recorded. The audio clips were edited to create customized lengths such that each acclimation session included audio from both sequences of increasing lengths and sound levels (refer to Table 1). Additionally, sound-suppression foam was adhered to the inner surfaces of the mock scanner box to reduce the noise that escaped the acclimation room (i.e., to prevent other studies in nearby spaces from being affected). The foam is a multi-layer acoustic suppression medium consisting of a high-density rubber base (approximately 2 mm) with a foam backing (approximately 5 mm).

2.7 MRI Acquisition

All acquisitions were performed at the Centre for Functional and Metabolic Mapping at Western University. MRI scans were acquired on a 9.4 T, 31-cm horizontal-bore magnet (Varian/Agilent, Yarnton, UK) with a 6-cm Magnex HD gradient insert and Bruker BioSpec Avance NEO console running ParaVision 360 v3.3 (Bruker BioSpin Corp, Billerica, MA).

Groups 1, 2, and 3 had four 10-minute functional runs acquired per session (TR=1.5 s, TE=12 ms, resolution=300x300x400 mm^3, slice gap=100 mm, matrix=64x32x30 voxels, 400 volumes). Following the functional scans, a T2-weighted Turbo RARE anatomical scan was acquired (TR=5.5 s, TE=30 ms, resolution=150x150x400 mm^3, slice gap=100 mm, 192x96x30 voxels, flip angle=160 degrees). Group 4 was acquired independently and had slightly different acquisition parameters. Namely, 2 functional runs were acquired per session with 600 volumes each (15-min runs). All other parameters were the same.

2.8 fMRI Analysis

All fMRI data were analyzed using the Rodent Automated Bold Improvement of EPI Sequences (RABIES version 0.5.1) (Desrosiers-Grégoire et al., 2024). All parameters used for RABIES processing stages are provided in Supplementary Table 1. Images were motion corrected using a trimmed mean across the acquired EPI frames in each run. They were then registered to a common space using an unbiased template as an intermediate step to improve registration (Avants et al., 2011). Image distortions due to susceptibility artifacts were corrected by nonlinearly registering EPI frames to the corresponding subject's T2w anatomical image (Wang et al., 2017). This is performed after first applying an inhomogeneity correction to all EPI frames. Importantly, all transformations calculated during preprocessing (from motion correction to registration and susceptibility correction) are concatenated and applied in a single operation to avoid multiple stages of resampling. Final common space images were resampled to 0.2 mm x 0.2 mm x 0.2 mm prior to further processing.

Frame censoring was carried out using a framewise displacement threshold of 0.15 mm. All frames exceeding this value, along with the preceding frame and the two following frames were removed (Power et al., 2012). If fewer than 200 volumes remained after censoring, the run was excluded from further analyses. Following this, data were detrended on a voxel-wise basis to remove linear drifts and converted to units of percent BOLD change through grand mean scaling (i.e., dividing by the grand mean signal and multiplying by 100). The 6 motion parameters calculated during motion correction were used as regressors to further clean the data. Lastly, spatial smoothing (Abraham et al., 2014) was implemented using a full-width half maximum value of 0.3 mm.

2.9 Motion Evaluation

Motion was estimated by registering EPI volumes and determining the displacements for each run. Although typical motion analyses involve measuring the 6 rigid body parameters, the voxel displacements between subsequent volumes are more important for data quality and better predict motion artifacts. This is because low frequency motion can be much more readily corrected for than high frequency spikes (Power et al., 2018; Soares et al., 2016). Here, we use the mean voxel-wise framewise displacement (FD) metric as performed in RABIES. It is calculated by taking the average of brain voxel displacements between each subsequent volume. A more detailed description of this metric can be found in the RABIES documentation (Desrosiers-Grégoire et al., 2024). This metric was used to compare motion levels between the 3 acclimatation protocols using the non-invasive restraint and the headpost restraint. The Kruskal-Wallis test was performed to determine significant differences followed by Bonferroni-corrected Wilcoxon rank sum test to determine which groups were significantly different.

2.10 Resting-State Network Analysis

Following preprocessing, fMRI data quality was analyzed to evaluate the performance of the non-invasive restraint. Due to the subjective nature of evaluating the robustness of resting-state networks, we decided to compare our data using an externally derived component representing the well-established somatomotor network (Pagani et al., 2023). This was done by running dual-regression on our data using the prior component and then using Permutation Analysis of Linear Models (PALM) (Winkler et al., 2014) to attain group statistical maps representing how much each group contains the prior component. The external networks were determined from two datasets comprising data from several institutions with a combined sample size of 366 animals (Desrosiers-Grégoire et al., 2024).

First, we compared the network differences between the 3 non-invasive restraint acclimation protocols and the headpost group using the prior component. To ensure the same amount of data was used, the total number of frames acquired in the headpost group was calculated and the same quantity of data was randomly selected from each non-invasive group (note this is prior to frame censoring). Group maps were then generated using PALM and z-scores were shown. To evaluate network quality, spatial specificity of the maps was measured using the Dice Similarity Coefficient (DSC) between the prior component with a z-threshold of 3.1 and the group map with a z-threshold of 3.0. The prior component threshold was chosen to represent a p value of 0.001 and the group map z threshold was selected to achieve the best overlap between the headpost group and the prior network. Multiple z values were tested to determine this optimal value. This same value was used for the non-invasive groups to fairly compare between groups. Additionally, the voxel-wise correspondence of z-values between the group and prior networks were obtained using the Pearson correlation coefficient (r) in the

region of the network (by masking both prior and group networks by the voxels in the prior network that were greater or equal to 3.1).

To understand the relative effects of motion and sample size on network specificity and amplitude correspondence (i.e. the z-score of a voxel in the prior map vs the z-score of the same voxel in the restraint group maps), the non-invasive data from each acclimation protocol were aggregated and separated into 5 groups according to the amount of motion present measured by the average run FD (namely motion group 1-5, Supplementary Table 2). Within each motion group, runs would be randomly sampled to form groups with 30, 60, 90, 120, 150, 180, and 210 minutes of acquisition. This was accomplished through bootstrapping (randomly sampling the data without replacement). For each group, 10 random samples were selected, and PALM was used to attain group maps. Network specificity was again evaluated using the DSC of the group map and the prior component map. Similar to the acclimation group comparison, a z-value threshold of 3.1 was used for the prior component (representing a p value of 0.001) and the z-value threshold of the group networks was 3.0. For each cumulative acquisition time, a one-way ANOVA was used to determine if groups significantly differed from one another. Tukey's test for multiple comparisons was then used to determine the specific groups that significantly differed.

The effects of cumulative group acquisition time and motion on network spatial specificity were further investigated by determining linear trendlines that represented the data in Supplementary Figure 1. All functional runs were aggregated and ranked by their average framewise displacement (FD) values, in ascending order of motion. Runs were grouped sequentially, starting with pairs, and the corresponding group map for each pair was generated. This map was then used to calculate the DSC. The process was repeated with progressively larger group sizes, including triplets, quartets, and so on, up to groups of ten (Supplementary Figure 1).

2.11 Stress response

Animal weight and video monitoring were used to assess stress of all mice throughout acclimation and scanning. A subset of mice (n = 21) was used to quantitatively assess corticosterone changes throughout the short (4-day), medium (9-day) and long (13-day) acclimation sessions. In contrast to the conventional extraction of CORT through blood serum which may cause a confounding stress response (Eleftheriou et al., 2020; Rowland & Toth, 2019; Russo et al., 2021), we employed extraction from fecal pellets similar to (Russo et al., 2021) This was performed by collecting the fecal pellets defecated during each session. CORT was extracted and the concentrations were determined using an ELISA following the supplier's manual (Arbor Assays DetectX Corticosterone Chemiluminescent Immunoassay Kit, catalog number K014-C). All concentrations were measured in duplicate and are expressed as ng of CORT per mg of fecal matter.

Corticosterone was analyzed on days 1, 2, and 4 for the 4-day protocol, days 1, 2, 4, and 9 for the 9-day protocol, and days 1, 2, 4, 9, and 13 for the 13-day protocol. All samples were read from a luminescence-capable plate reader (SpectraMax® M5 Multimode Plate Reader, Molecular Devices, USA). One-way ANOVA was used to compare CORT concentrations in each acclimation group. No corticosterone analysis was performed on the headpost group as it was a dataset acquired previously for a separate study. However, corticosterone data from head fixed animals using similar headposts has been obtained by others (Lindhardt et al., 2022).

3 Results

3.1 Motion Evaluation

We first analysed scan motion levels to determine if motion depends on the acclimation protocol used (Figure *2*). The framewise displacement for each voxel was measured and the average across each run was computed. Figure *2* (a) shows a representative motion plot with the 6 rigid body parameters (3 translations – top, and 3 rotations – middle). The corresponding mean voxel-wise displacements are shown below in Figure *2* (a). A histogram is plotted in Figure *2* (b) showing all FD measures for all acquired volumes. This metric was then used in Figure *2* (c) to compare motion between cohorts. Motion was significantly higher in the 4-day group than the 9-day group, and motion was significantly lower in the headpost group than all other groups. Note, after censoring, 12.5% of the total number of acquired volumes were censored and 19 of the 226 runs were excluded due to being left with fewer than 200 volumes after censoring. A comprehensive comparison of the censored volumes based on group can be found in Supplementary Table *2*.

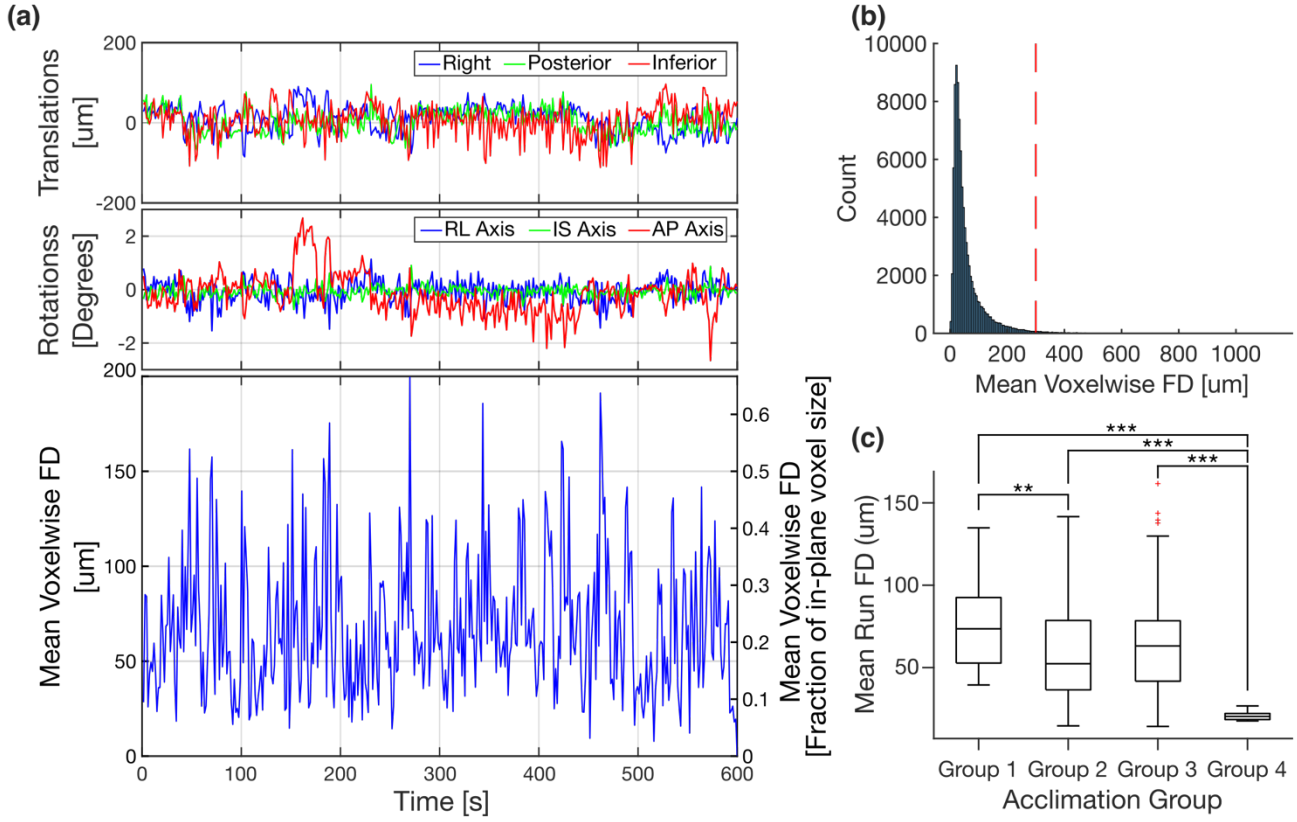

Figure 2. Scan motion levels for the different restraints and acclimation protocols. (a) Representative plot displaying the motion parameters (3 translations – top, 3 rotations – middle, and the corresponding mean voxel-wise framewise displacements – bottom). The plot is expressed in FD magnitude (left y-axis) and as a fraction of the in-plane voxel size (300 μm – right y-axis). (b) A histogram displaying mean voxel-wise FD values for all volumes in a run (e.g., the mean value of FD values displayed in (b) bottom) for all subjects. The red vertical line indicates the in-plane voxel size (300 μm). (c) Boxplots comparing the motion between the four cohorts. Outliers are shown as red '+'. The mean run voxel-wise FD values are calculated by taking the average of brain voxel displacements between each subsequent volume (* = $p < 0.05$, ** = $p < 0.01$, *** = $p < 0.001$, Kruskal-Wallis rank sum test followed by Bonferroni-corrected Wilcoxon rank sum test).

3.2 Resting-State Networks

To avoid the bias of using components generated from this dataset and promote standardization across centres, dual regression was performed using previously generated components through independent component analysis that established well-known resting-state networks (Desrosiers-Grégoire et al., 2024). To confirm the networks are recoverable in our datasets, dual regression of the somatomotor network was performed for each scan and data were grouped by acclimation group (Figure *3*). The DSC representing the amount of overlap and correlation coefficient representing the amplitude correspondence between the networks is overlaid above each network. Note, only a sample slice is shown however the DSC and correlation coefficients were calculated from the entire volume.

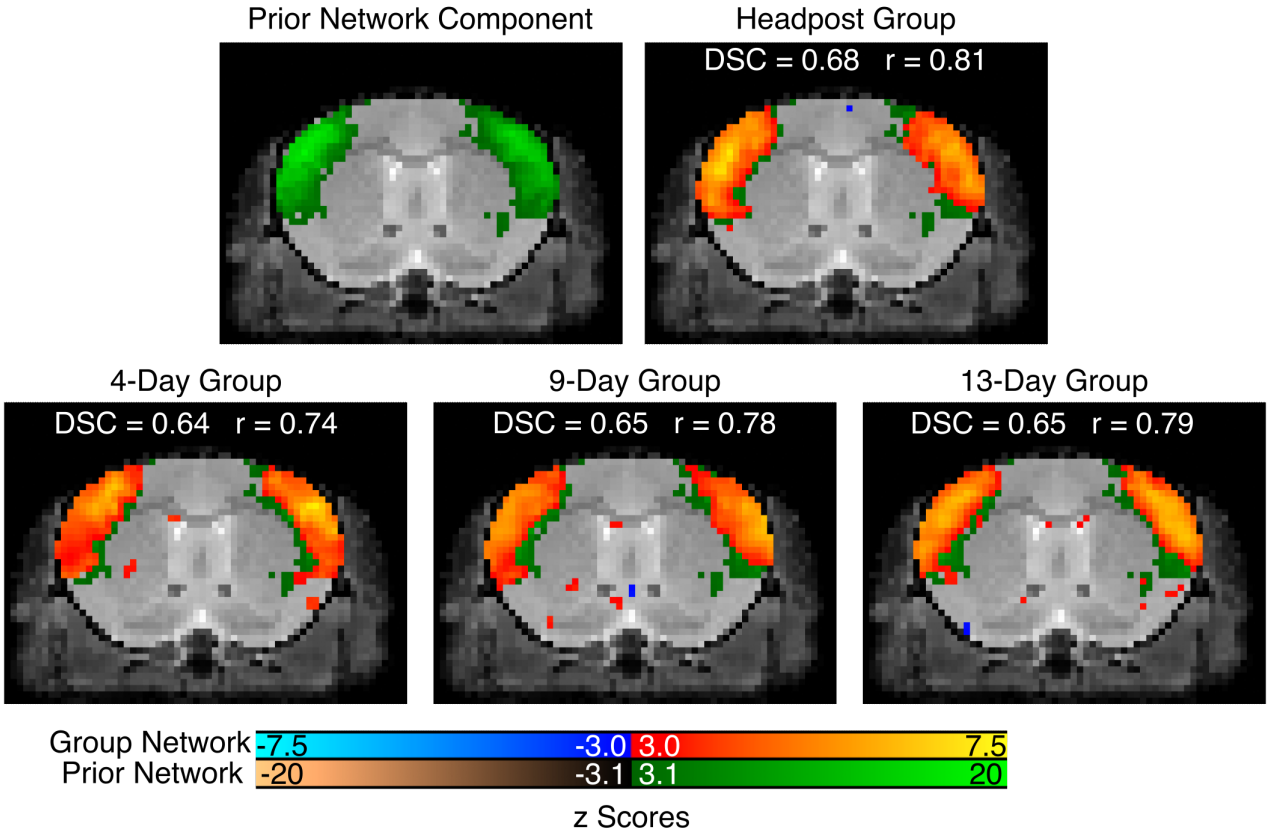

Figure 3. Network quality comparison of the 3 non-invasive protocols and the headpost group using the Dice Similarity Coefficient (DSC) and amplitude correspondence (using the Pearson correlation coefficient, r) with the externally derived somatomotor component (Desrosiers-Grégoire et al., 2024). Note, DSC and correlation values were calculated using the whole volume but only one sample slice is shown. The top left network map shows the externally derived component. The top right shows the contribution in the headpost group overlayed on top of the prior component. The bottom row shows the same comparison except for the 4-Day, 9-Day and 13-Day groups, respectively. Corresponding DSC and r values are annotated over each network.

We further investigated the relationship between motion, sample size and network quality by looking at how varying levels of motion and cumulative group acquisition time affect quality (i.e., DSC and amplitude correlation) relative to the prior network component (Figure *4*). Refer to Supplementary Figure *2* to see the resulting correlation results for a single sample from each motion level and cumulative acquisition time. Past 120 min of acquired data, both DSC and amplitude correlation analyses show clear statistical differences between headpost

and non-invasive groups. Taking this a step further, all functional runs were aggregated and ranked by their average framewise displacement (FD) values, in ascending order of motion. Runs were grouped sequentially, starting with pairs, and the corresponding group map for each pair was generated. This map was then used to calculate the DSC. The process was repeated with progressively larger group sizes, including triplets, quartets, and so on, up to groups of ten.

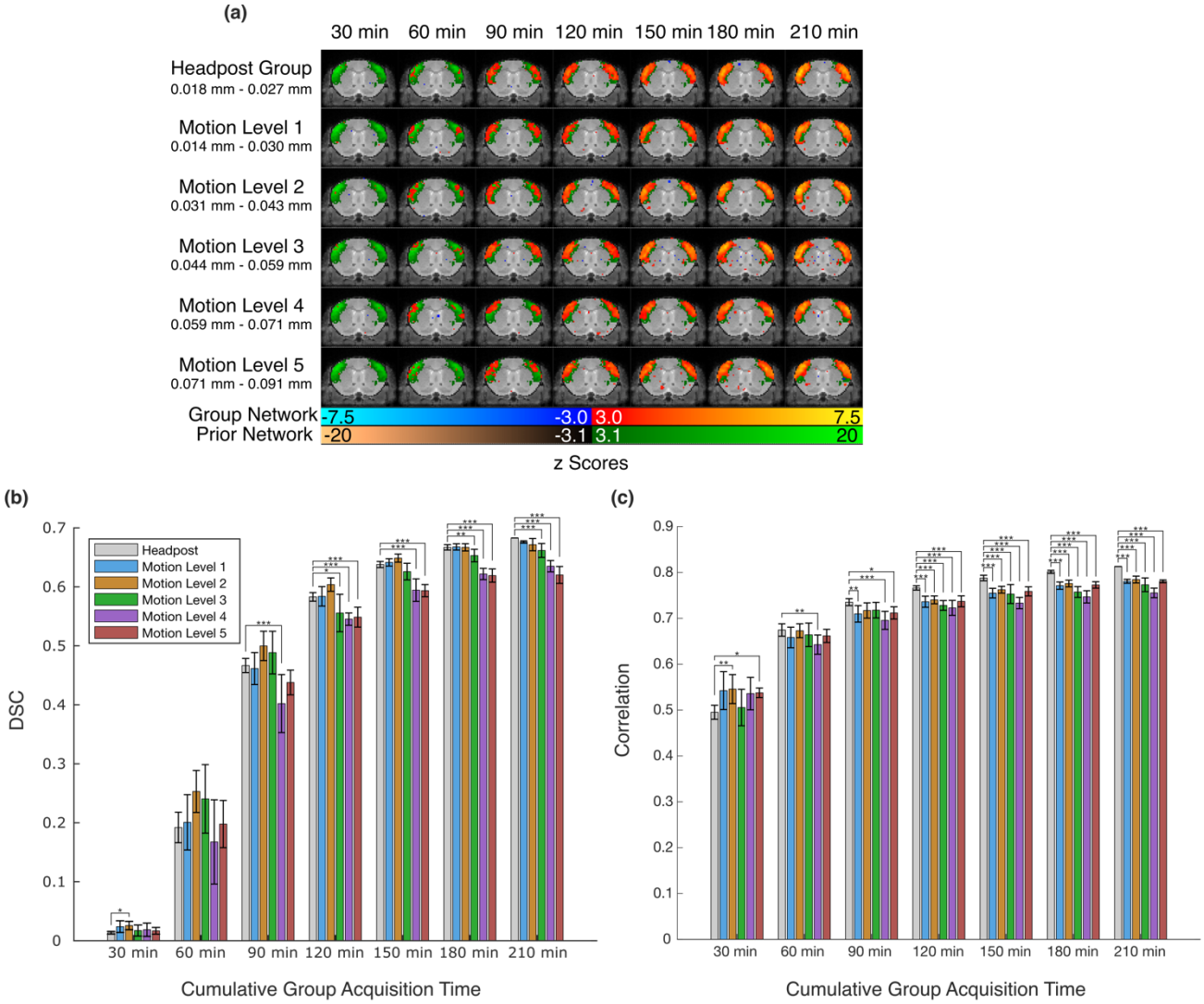

Figure 4. Group network quality assessment for the headpost and aggregated non-invasive data relative to the prior network component. Groups have varying levels of motion and cumulative acquisition time. (a) Sample slices of the z-maps of the prior component (z values between 3.1 and 20 illustrated in green/brown) and the group network (z values of 3.0 to 7.5 illustrated in red/blue). Motion Level 1 indicates the lowest amount of motion and Motion Level 5 indicates high motion. The range of average FD values for each group are displayed below each Motion Level on the left. (b) Corresponding Dice Similarity Coefficient (DSC) values to the network overlaps shown in (a). (c) Correspondence of z-values compared voxel-wise between the prior map and the group map masked to include voxels in the prior network region. Error bars in (b) and (c) represent the standard deviation of 10 random samples selected from the respective group. Groups that significantly differed from the headpost group for each cumulative acquisition time are shown (* = $p < 0.05$, ** = $p < 0.01$, *** = $p < 0.001$, for Tukey's test for multiple comparisons following one-way ANOVA).

3.3 Stress

Mouse stress was approximated using weight loss and fecal corticosterone concentration over the course of the acclimation sessions. Weight was measured each day of

acclimation. Values were normalized to the weight on day 1 and plotted for each cohort separately (Figure *5* (a) and (b)). Paired t-tests were conducted to test for statistical differences between first and last days of acclimation for each group. Headpost, 9-day and 13-day groups all had significant weight losses. However, the headpost group only showed a significant difference when both sexes were aggregated. When males and females were analyzed separately, no significant difference was found (Supplementary Figure 3). Fecal corticosterone metabolite (FCM) was measured from a subset of mice from each non-invasive group. Results are shown in Figure *5* (c) and Supplementary Figure 3 (c) and (d). Note, the headpost group was acquired previously and fecal samples were not collected. One-way ANOVA was conducted. Paired t-tests could not be performed since several groups had missing samples (due to the subject not defecating during the respective acclimation session). There was no significant difference in corticosterone levels between sampling days across the acclimation protocols.

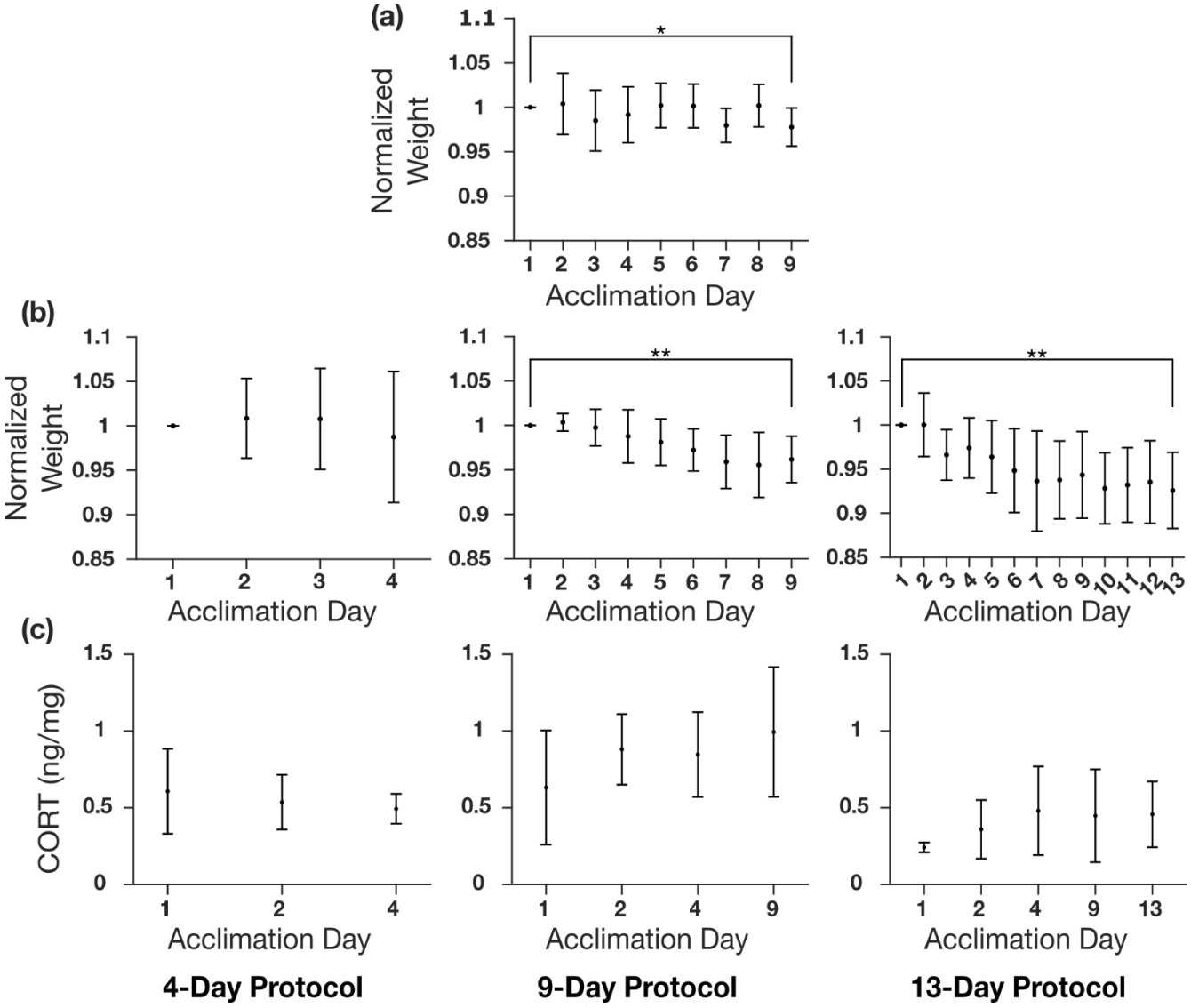

Figure 5. Weight and fecal corticosterone changes across acclimation sessions. (a) Weight changes for all subjects (n = 7) in the headpost group normalized to the weight on day 1. The weight on the last day is significantly less than the first day (paired t-test, $p < 0.05$). (b) Weight changes of all subjects in the 4-day, 9-day and 13-day groups over the course of the different acclimation lengths normalized to the weight on day 1. Note the headpost group underwent the same 9-day

acclimation session as the 9-day non-invasive group. Both the 9-day group and 13-day group showed significant weight decreases (paired t-test, $p < 0.01$). (c) Corticosterone concentration changes over the course of the three acclimation durations. Note, the headpost group was acquired in a separate study and corticosterone samples were not collected. There were no significant CORT changes across acclimation sessions (one-way ANOVA, $p > 0.05$).

4 Discussion

All subjects used in the current study successfully used the restraint and accompanying acclimation protocols. The restraint contains several adjustable features to tailor the fit for each mouse regardless of size (i.e., 16 – 37 g as tested here). Similar to previous non-invasive restraints (Madularu et al., 2017), our restraint is 3D printed and modular in nature allowing for easy modification. Furthermore, no anesthesia is required for setup and experienced handlers can position acclimated mice in less than 5 min.

Three different acclimation procedures were developed representing a range of protocols typically found in recent awake mouse MRI literature (see (Mandino et al., 2023; Zeng et al., 2022) for comprehensive acclimation protocol comparisons). Based on our motion analysis, mice in the 4-day protocol did move significantly more than the 9-day group. Indeed, 20.6% of volumes were censored and 13.9% of runs were excluded due to being above the motion threshold (Supplementary Table 2). Even so, the network specificity between the 4-day and 9-day groups were almost identical at 0.64 and 0.65, respectively. Similarly, the 13-day group also had a spatial specificity of 0.65 and did not significantly differ in motion compared to the other two groups.

Non-invasive restraints are more vulnerable to residual motion compared to headpost restraints, since the latter directly fixates the skull. However, we have found the impact of the motion confound reduces tremendously with increased sample size as demonstrated in Figure *4*. Since motion tends to affect a relatively constant proportion of data, an increased sample size will allow for increased statistical power after censoring of motion-affected frames. Even at the extreme end, in untrained young human subjects, Smith and colleagues evaluated how harmful this motion is to data quality using similar metrics outlined here. In the end, they conclude a conservative design would be to acquire 2 to 3 times more data than would be expected for the same study without high-motion subjects (Smith et al., 2022). Our data suggest a much lower quantity of data is required. Despite allowing more than 3x the motion than the headpost cohort (Figure *2* (c)), acquiring 25% more data with the non-invasive restraint will compensate for censored volumes assuming most motion is at the high end allowed by the restraint.

The effects of motion are only seen past 50 min of cumulative group acquisition time. From Supplementary Figure 1, this is evident from the emergence of the negative slope of the linear trendlines. The slope only becomes noticeable in the 50 min group and above. The groups with less cumulative acquisition time contain other sources of variation such that the effects of motion are not apparent. Individual network variability can cause such variation (Bergmann et al., 2020; Fu et al., 2023). Similarly, in Figure 4 the effects of motion are only seen at 90 min as can be seen by the lower spatial specificity for motion groups 4 and 5 – though it is only apparent between the headpost group and the lower motion groups at higher amounts of data when the other sources of variation are presumably averaged out.

Sample size is a current topic of controversy among animal imaging researchers (Grandjean et al., 2024; Mandino et al., 2023). There is motivation from an ethics perspective to use smaller sample sizes, whereas from a statistical perspective, large sample sizes are preferred. Fortunately, here the slightly higher motion corrupted data benefits the same amount from increased group cumulative acquisition time compared to the headpost restraint (Figure *4*, Supplementary Figure 1). For instance, past 2 hours of cumulative acquisition time, all groups have a spatial specificity above 0.5 (Figure 4 (b)) and an amplitude correspondence greater than 0.7 (Figure 4 (c)). The results indicate the amount of data is much more important than the amount of motion during the acquisition. Indeed, with long cumulative acquisition times

(approaching 210 min), the spatial specificity difference between motion groups seems to be solely based on the number of frames censored. It is possible higher amounts of motion (i.e., greater than the in-plane voxel size) would further degrade the networks, but that was not investigated here as almost all (98.7%) displacements were under the in-plane voxel size (Figure 2 (b)). Surprisingly, we do not see this same relationship when looking at the amplitude correspondence. Approaching higher cumulative group acquisition times, the headpost group emerges with a statistically significant increase over all non-invasive motion level groups, however no clear relationship emerges among motion level groups like we see in the spatial specificity analyses. This suggests that this amplitude correspondence metric is independent of motion, at least at the levels observed here. However, increased cumulative acquisition time still increases correlation values of all groups indicating differences between the headpost and non-invasive restraint can be addressed by simply acquiring more data.

Stress has been shown to be a critical measure for awake fMRI as it has been shown to impact functional connectivity (Grandjean et al., 2016; Maron-Katz et al., 2016). There is a statistically significant weight loss between the first and last days of acclimation in the headpost group, and the 9-day and 13-day non-invasive groups. Although no loss is observed in the 4-day group, this is likely because the 4-day duration is too short to observe the change. Although these weight losses are statistically significant, they remain below the critical threshold of 15%, which is considered a concern for animal welfare by most animal care committees.

FCM was measured and compared for several selected days throughout each non-invasive acclimation group. Specifically, fecal samples were used over serum samples to minimize unrelated stress to the animals (Kroll et al., 2021). For the same reason, day 1 was selected as our baseline as it is well known that CORT is only detectable in feces hours after the stressful event (Rowland & Toth, 2019). It is also sensible to assume the FCM measurement on Day 1 is in fact a baseline measurement because 1) any CORT would not be detectable within 20 min (maximum duration between stress event onset and fecal excretion) of the stressor, and 2) the procedure on day 1 is the least stressful and likely would not result in any significant increase in CORT (e.g., Lindhardt et al. demonstrated that even a more intensive protocol involving 20 minutes of restraint on Day 1 did not result in a significant increase in corticosterone (Lindhardt et al., 2022)).

Surprisingly, no significant change in corticosterone concentration was observed in any of the acclimation groups. Consequently, these results would indicate no relationship between acclimation session and stress in mice and stress would not explain the observed difference in motion between the 4-day and 9-day acclimation groups. This is an unexpected result compared to the literature (Ferris et al., 2011; Gutierrez-Barragan et al., 2022; Lindhardt et al., 2022; Low et al., 2016). This could be due to the measurement of FCM rather than more acutely sensitive measures of CORT such as through plasma samples. FCM is known to integrate the CORT levels over relatively long periods of time (hours to days) (Rowland & Toth, 2019). It is possible our maximum 1.5-hour stressor did not produce a detectable CORT increase over the 48-hour integration time. (Lindhardt et al., 2022) used fecal corticosterone measurements and did find a difference on day 11 of acclimation compared to day 1. However, they used a more aggressive acclimation protocol than used here, therefore it is possible the animals showed a larger stress increase on the first few days. Those animals also underwent surgery which imposes an additional variable to consider.

Due to the results of this study, along with indications from related literature, the authors recommend future corticosterone experiments be acquired over longer durations each session. That is to say that single time-point measurements of CORT can be misleading and are difficult to interpret. Further, it should be noted that it is still not fully understood what increases in

corticosterone represent and indeed, corticosterone levels naturally vary widely dependent on many factors (Rowland & Toth, 2019). While it is generally thought that increases correspond with increases in negative stress, it has also been postulated that elevations in HPA and basal glucocorticoid levels may be linked with stress adaptation, a positive outcome rather than excess stress (Rowland & Toth, 2019). More stress-targeted studies are required to both characterize and better understand the relationship of corticosterone concentration on perceived stress.

4.1 Limitations

Like all T2*-weighted sequences, care should be taken to minimize the effect of all major sources of susceptibility artifacts. This includes avoiding the use of magnetic materials and avoid pockets of air near tissue. One such source relevant to the proposed restraint was the susceptibility artifact caused by the ears of the mouse. Since the posterior arch can fold the ears onto the head, care should be taken to ensure the ears are folded towards the posterior and lateral regions of the head rather than anterior and medial.

Another limitation is only one network (i.e., cortical somatomotor network) was used for network spatial specificity and amplitude correspondence measures. It is possible other cortical networks or even subcortical networks would have different results.

Although the restraint is designed to allow for tasks to be readily performed, task-based imaging was not conducted in the current study. It can be postulated that tasks may cause task-induced motion, the effects of which are amplified in restraints allowing for increased baseline levels of motion. However, since resting-state networks were clearly identifiable, it is likely task-based networks will only be clearer due to the higher activation and statistical power associated with task-based protocols (Zhao et al., 2023). An additional limitation of this work is it does not consider intra-volume motion. Consequently, acquisitions with large movements that occur and return to the original position during the same TR may not be robustly corrected and can also have degrading effects (Kim et al., 1999) which may explain some of the variance observed in the network spatial specificity analyses. Lastly, this study focused on the network measures using group ICA-based analyses. Although this is a very common approach used in resting-state fMRI studies, investigation into the effects of motion and cumulative group data quantity on other resting-state analysis approaches including seed-based and connectivity matrix-based approaches were not conducted.

5 Conclusion

A non-invasive restraint was developed and evaluated along with three different acclimation protocols. After evaluating motion and network quality with an externally generated well-established network, the acclimation protocol was not found to change network spatial specificity despite the short 4-day acclimation group having increased motion. However, longer acclimation protocols (9-day and 13-day) did have improved amplitude correspondence with the prior network. Separately analyzing the effect of motion and amount of data on network quality showed a relatively small effect of motion compared to the large effect of amount of data indicating increasing amount of scanning time (at the group and subject levels) is much more important than the motion contamination allowed by the proposed approach. Invasive headpost restraints have pushed the mouse fMRI field forward tremendously allowing for awake scanning with very little motion. However, to increase translational utility, more focus should be put on the development of non-invasive restraints to better align with scanning practices in humans. By acquiring approximately 25% more data to conservatively compensate for censoring of high motion frames, group resting state networks can be acquired at comparable quality to headpost approaches. The proposed restraint is useful especially in situations where high-throughput scanning is required without the use of any anesthesia for subject positioning, and if ample unobstructed skull access is necessary, e.g., for multi-modal electrophysiology/optical/fMRI studies. This awake MRI approach represents a step forward in increased translational utility between mouse and human neuroimaging.

Data and Code Availability

All data and code have been made freely available (https://doi.org/10.17605/OSF.IO/TYHCE).

Author Contributions

S.L., and R.M. designed the study, S.L., A.E., M.B., and M.N. collected and analyzed the data, S.L., K.M.G., P.Z., and R.M. designed the non-invasive restraint, S.L. wrote the initial draft of the manuscript with feedback and review from all authors.

Funding

This work was supported by funding from the Canadian Institutes for Health Research (FDN-148453), a Brain Canada Platform Support Grant and a Canada First Research Excellence Fund award to BrainsCAN and a New Frontiers in Research Fund Transformation award (NFRFT-2022-00051).

Declaration of Competing Interests

Nothing to declare.

Acknowledgements

We thank Alex Li for his help setting up and troubleshooting MRI scans; Gabriel Desrosiers-Grégoire, Gabriel A. Devenyi, and Mallar Chakravarty from The Douglas Research Centre for technical assistance with RABIES; and the Animal Care Committee from Western University and veterinarians for feedback and suggestions while developing the non-invasive restraint.

References

Abraham, A., Pedregosa, F., Eickenberg, M., Gervais, P., Mueller, A., Kossaifi, J., Gramfort, A., Thirion, B. & Varoquaux, G. (2014). Machine learning for neuroimaging with scikit-learn. *Frontiers in Neuroinformatics*, *8*, 14. https://doi.org/10.3389/fninf.2014.00014

Avants, B. B., Tustison, N. J., Song, G., Cook, P. A., Klein, A. & Gee, J. C. (2011). A reproducible evaluation of ANTs similarity metric performance in brain image registration. *NeuroImage*, *54*(3), 2033–2044. https://doi.org/10.1016/j.neuroimage.2010.09.025

Bergmann, E., Gofman, X., Kavushansky, A. & Kahn, I. (2020). Individual variability in functional connectivity architecture of the mouse brain. *Communications Biology*, *3*(1), 738. https://doi.org/10.1038/s42003-020-01472-5

Chen, X., Tong, C., Han, Z., Zhang, K., Bo, B., Feng, Y. & Liang, Z. (2020). Sensory evoked fMRI paradigms in awake mice. *NeuroImage*, *204*, 116242. https://doi.org/10.1016/j.neuroimage.2019.116242

Desjardins, M., Kılıç, K., Thunemann, M., Mateo, C., Holland, D., Ferri, C. G. L., Cremonesi, J. A., Li, B., Cheng, Q., Weldy, K. L., Saisan, P. A., Kleinfeld, D., Komiyama, T., Liu, T. T., Bussell, R., Wong, E. C., Scadeng, M., Dunn, A. K., Boas, D. A., … Devor, A. (2019). Awake Mouse Imaging: From Two-Photon Microscopy to Blood Oxygen Level–Dependent Functional Magnetic Resonance Imaging. *Biological Psychiatry: Cognitive Neuroscience and Neuroimaging*, *4*(6), 533–542. https://doi.org/10.1016/j.bpsc.2018.12.002

Desrosiers-Grégoire, G., Devenyi, G. A., Grandjean, J. & Chakravarty, M. M. (2024). A standardized image processing and data quality platform for rodent fMRI. *Nature Communications*, *15*(1), 6708. https://doi.org/10.1038/s41467-024-50826-8

Dinh, T. N. A., Jung, W. B., Shim, H.-J. & Kim, S.-G. (2021). Characteristics of fMRI responses to visual stimulation in anesthetized vs. awake mice. *NeuroImage*, *226*, 117542. https://doi.org/10.1016/j.neuroimage.2020.117542

Eleftheriou, A., Palme, R. & Boonstra, R. (2020). Assessment of the Stress Response in North American Deermice: Laboratory and Field Validation of Two Enzyme Immunoassays for Fecal Corticosterone Metabolites. *Animals*, *10*(7), 1120. https://doi.org/10.3390/ani10071120

Ellenbroek, B. & Youn, J. (2016). Rodent models in neuroscience research: is it a rat race? *Disease Models & Mechanisms*, *9*(10), 1079–1087. https://doi.org/10.1242/dmm.026120

Fadel, L. C., Patel, I. V., Romero, J., Tan, I.-C., Kesler, S. R., Rao, V., Subasinghe, S. A. A. S., Ray, R. S., Yustein, J. T., Allen, M. J., Gibson, B. W., Verlinden, J. J., Fayn, S., Ruggiero, N., Ortiz, C., Hipskind, E., Feng, A., Iheanacho, C., Wang, A. & Pautler, R. G. (2022). A Mouse Holder for Awake Functional Imaging in Unanesthetized Mice:

Applications in 31P Spectroscopy, Manganese-Enhanced Magnetic Resonance Imaging Studies, and Resting-State Functional Magnetic Resonance Imaging. *Biosensors*, *12*(8), 616. https://doi.org/10.3390/bios12080616

Ferris, C. F. (2022). Applications in Awake Animal Magnetic Resonance Imaging. *Frontiers in Neuroscience*, *16*, 854377. https://doi.org/10.3389/fnins.2022.854377

Ferris, C. F., Smerkers, B., Kulkarni, P., Caffrey, M., Afacan, O., Toddes, S., Stolberg, T. & Febo, M. (2011). Functional magnetic resonance imaging in awake animals. *Reviews in the Neurosciences*, *22*(6), 665–674. https://doi.org/10.1515/rns.2011.050

Fu, Z., Liu, J., Salman, M. S., Sui, J. & Calhoun, V. D. (2023). Functional connectivity uniqueness and variability? Linkages with cognitive and psychiatric problems in children. *Nature Mental Health*, *1*(12), 956–970. https://doi.org/10.1038/s44220-023-00151-8

Gao, Y.-R., Ma, Y., Zhang, Q., Winder, A. T., Liang, Z., Antinori, L., Drew, P. J. & Zhang, N. (2017). Time to wake up: Studying neurovascular coupling and brain-wide circuit function in the un-anesthetized animal. *NeuroImage*, *153*, 382–398. https://doi.org/10.1016/j.neuroimage.2016.11.069

Grandjean, J., Azzinnari, D., Seuwen, A., Sigrist, H., Seifritz, E., Pryce, C. R. & Rudin, M. (2016). Chronic psychosocial stress in mice leads to changes in brain functional connectivity and metabolite levels comparable to human depression. *NeuroImage*, *142*, 544–552. https://doi.org/10.1016/j.neuroimage.2016.08.013

Grandjean, J., Lake, E. M. R., Pagani, M. & Mandino, F. (2024). What N Is N-ough for MRI-Based Animal Neuroimaging? *ENeuro*, *11*(3), ENEURO.0531-23.2024. https://doi.org/10.1523/eneuro.0531-23.2024

Gutierrez-Barragan, D., Singh, N. A., Alvino, F. G., Coletta, L., Rocchi, F., Guzman, E. D., Galbusera, A., Uboldi, M., Panzeri, S. & Gozzi, A. (2022). Unique spatiotemporal fMRI dynamics in the awake mouse brain. *Current Biology*. https://doi.org/10.1016/j.cub.2021.12.015

Harris, A. P., Lennen, R. J., Marshall, I., Jansen, M. A., Pernet, C. R., Brydges, N. M., Duguid, I. C. & Holmes, M. C. (2015). Imaging learned fear circuitry in awake mice using fMRI. *European Journal of Neuroscience*, *42*(5), 2125–2134. https://doi.org/10.1111/ejn.12939

Kim, B., Boes, J. L., Bland, P. H., Chenevert, T. L. & Meyer, C. R. (1999). Motion correction in fMRI via registration of individual slices into an anatomical volume. *Magnetic Resonance in Medicine*, *41*(5), 964–972. https://doi.org/10.1002/(sici)1522-2594(199905)41:5<964::aid-mrm16>3.0.co;2-d

Kroll, T., Kornadt-Beck, N., Oskamp, A., Elmenhorst, D., Touma, C., Palme, R. & Bauer, A. (2021). Additional Assessment of Fecal Corticosterone Metabolites Improves Visual Rating in the Evaluation of Stress Responses of Laboratory Rats. *Animals*, *11*(3), 710. https://doi.org/10.3390/ani11030710

Lindhardt, T. B., Gutiérrez-Jiménez, E., Liang, Z. & Hansen, B. (2022). Male and Female C57BL/6 Mice Respond Differently to Awake Magnetic Resonance Imaging Habituation. *Frontiers in Neuroscience*, *16*, 853527. https://doi.org/10.3389/fnins.2022.853527

Low, L. A., Bauer, L. C., Pitcher, M. H. & Bushnell, M. C. (2016). Restraint training for awake functional brain scanning of rodents can cause long-lasting changes in pain and stress responses. *PAIN*, *157*(8), 1761–1772. https://doi.org/10.1097/j.pain.0000000000000579

Madularu, D., Mathieu, A. P., Kumaragamage, C., Reynolds, L. M., Near, J., Flores, C. & Rajah, M. N. (2017). A non-invasive restraining system for awake mouse imaging. *Journal of Neuroscience Methods*, *287*, 53–57. https://doi.org/10.1016/j.jneumeth.2017.06.008

Mandino, F., Cerri, D. H., Garin, C. M., Straathof, M., Tilborg, G. A. F. van, Chakravarty, M. M., Dhenain, M., Dijkhuizen, R. M., Gozzi, A., Hess, A., Keilholz, S. D., Lerch, J. P., Shih, Y.-Y. I. & Grandjean, J. (2020). Animal Functional Magnetic Resonance Imaging: Trends and Path Toward Standardization. *Frontiers in Neuroinformatics*, *13*, 78. https://doi.org/10.3389/fninf.2019.00078

Mandino, F., Vrooman, R. M., Foo, H. E., Yeow, L. Y., Bolton, T. A. W., Salvan, P., Teoh, C. L., Lee, C. Y., Beauchamp, A., Luo, S., Bi, R., Zhang, J., Lim, G. H. T., Low, N., Sallet, J., Gigg, J., Lerch, J. P., Mars, R. B., Olivo, M., … Grandjean, J. (2021). A triple-network organization for the mouse brain. *Molecular Psychiatry*, 1–8. https://doi.org/10.1038/s41380-021-01298-5

Mandino, F., Vujic, S., Grandjean, J. & Lake, E. M. R. (2023). Where do we stand on fMRI in awake mice? *Cerebral Cortex*, bhad478. https://doi.org/10.1093/cercor/bhad478

Maron-Katz, A., Vaisvaser, S., Lin, T., Hendler, T. & Shamir, R. (2016). A large-scale perspective on stress-induced alterations in resting-state networks. *Scientific Reports*, *6*(1), 21503. https://doi.org/10.1038/srep21503

Pagani, M., Gutierrez-Barragan, D., Guzman, A. E. de, Xu, T. & Gozzi, A. (2023). Mapping and comparing fMRI connectivity networks across species. *Communications Biology*, *6*(1), 1238. https://doi.org/10.1038/s42003-023-05629-w

Parker, C. C., Chen, H., Flagel, S. B., Geurts, A. M., Richards, J. B., Robinson, T. E., Woods, L. C. S. & Palmer, A. A. (2014). Rats are the smart choice: Rationale for a renewed focus on rats in behavioral genetics. *Neuropharmacology*, *76*, 250–258. https://doi.org/10.1016/j.neuropharm.2013.05.047

Power, J. D., Barnes, K. A., Snyder, A. Z., Schlaggar, B. L. & Petersen, S. E. (2012). Spurious but systematic correlations in functional connectivity MRI networks arise from subject motion. *NeuroImage*, *59*(3), 2142–2154. https://doi.org/10.1016/j.neuroimage.2011.10.018

Power, J. D., Plitt, M., Gotts, S. J., Kundu, P., Voon, V., Bandettini, P. A. & Martin, A. (2018). Ridding fMRI data of motion-related influences: Removal of signals with distinct spatial and

physical bases in multiecho data. *Proceedings of the National Academy of Sciences*, *115*(9), E2105–E2114. https://doi.org/10.1073/pnas.1720985115

Rowland, N. E. & Toth, L. A. (2019). Analytic and Interpretational Pitfalls to Measuring Fecal Corticosterone Metabolites in Laboratory Rats and Mice. *Comparative Medicine*, *69*(5), 337–349. https://doi.org/10.30802/aalas-cm-18-000119

Russo, G., Helluy, X., Behroozi, M. & Manahan-Vaughan, D. (2021). Gradual Restraint Habituation for Awake Functional Magnetic Resonance Imaging Combined With a Sparse Imaging Paradigm Reduces Motion Artifacts and Stress Levels in Rodents. *Frontiers in Neuroscience*, *15*, 805679. https://doi.org/10.3389/fnins.2021.805679

Smith, J., Wilkey, E., Clarke, B., Shanley, L., Men, V., Fair, D. & Sabb, F. W. (2022). Can this data be saved? Techniques for high motion in resting state scans of first grade children. *Developmental Cognitive Neuroscience*, *58*, 101178. https://doi.org/10.1016/j.dcn.2022.101178

Soares, J. M., Magalhães, R., Moreira, P. S., Sousa, A., Ganz, E., Sampaio, A., Alves, V., Marques, P. & Sousa, N. (2016). A Hitchhiker's Guide to Functional Magnetic Resonance Imaging. *Frontiers in Neuroscience*, *10*, 515. https://doi.org/10.3389/fnins.2016.00515

Szilagyi, K., Zieger, M. A., Li, J. & Kacena, M. A. (2018). Improving Post-Operative Outcomes in Aged and Diabetic Obese Mice. *Laboratory Animal Science Professional*, *6*(3), 65–67.

Takata, N., Sugiura, Y., Yoshida, K., Koizumi, M., Hiroshi, N., Honda, K., Yano, R., Komaki, Y., Matsui, K., Suematsu, M., Mimura, M., Okano, H. & Tanaka, K. F. (2018). Optogenetic astrocyte activation evokes BOLD fMRI response with oxygen consumption without neuronal activity modulation. *Glia*, *66*(9), 2013–2023. https://doi.org/10.1002/glia.23454

Wang, S., Peterson, D. J., Gatenby, J. C., Li, W., Grabowski, T. J. & Madhyastha, T. M. (2017). Evaluation of Field Map and Nonlinear Registration Methods for Correction of Susceptibility Artifacts in Diffusion MRI. *Frontiers in Neuroinformatics*, *11*, 17. https://doi.org/10.3389/fninf.2017.00017

Winkler, A. M., Ridgway, G. R., Webster, M. A., Smith, S. M. & Nichols, T. E. (2014). Permutation inference for the general linear model. *NeuroImage*, *92*(100), 381–397. https://doi.org/10.1016/j.neuroimage.2014.01.060

Wu, T., Wang, X., Zhang, R., Jiao, Y., Yu, W., Su, D., Zhao, Y. & Tian, J. (2020). Mice with pre-existing tumors are vulnerable to postoperative cognitive dysfunction. *Brain Research*, *1732*, 146650. https://doi.org/10.1016/j.brainres.2020.146650

Xu, N., LaGrow, T. J., Anumba, N., Lee, A., Zhang, X., Yousefi, B., Bassil, Y., Clavijo, G. P., Sharghi, V. K., Maltbie, E., Meyer-Baese, L., Nezafati, M., Pan, W.-J. & Keilholz, S. (2022). Functional Connectivity of the Brain Across Rodents and Humans. *Frontiers in Neuroscience*, *16*, 816331. https://doi.org/10.3389/fnins.2022.816331

Xu, W., Pei, M., Zhang, K., Tong, C., Bo, B., Feng, J., Zhang, X.-Y. & Liang, Z. (2022). A systematically optimized awake mouse fMRI paradigm. *BioRxiv*, 2022.11.16.516376. https://doi.org/10.1101/2022.11.16.516376

Zeng, H., Jiang, Y., Beer-Hammer, S. & Yu, X. (2022). Awake Mouse fMRI and Pupillary Recordings in the Ultra-High Magnetic Field. *Frontiers in Neuroscience*, *16*, 886709. https://doi.org/10.3389/fnins.2022.886709

Zhao, W., Makowski, C., Hagler, D. J., Garavan, H. P., Thompson, W. K., Greene, D. J., Jernigan, T. L. & Dale, A. M. (2023). Task fMRI paradigms may capture more behaviorally relevant information than resting-state functional connectivity. *NeuroImage*, *270*, 119946. https://doi.org/10.1016/j.neuroimage.2023.119946

Supplementary Figures and Tables

Supplementary Table 1. RABIES (version 0.5.1) processing stage commands.

Processing Stage	Parameters
Preprocessing	--anat_robust_inho_cor apply=true,masking=false,brain_extraction=false,template_registration=SyN --commonspace_resampling 0.2x0.2x0.2 --bold2anat_coreg masking=true,brain_extraction=false,registration=SyN
Confound Correction	--smoothing_filter 0.3 --conf_list mot_6 --frame_censoring FD_censoring=true,FD_threshold=0.15,DVARS_censoring=false,minimum_timepoint=200
Analysis	--data_diagnosis

Supplementary Table 2. Percentage of volumes censored for each group. The first 4 rows represent the data divided based on acclimation group. The last 6 rows represent the non-invasive data grouped by average framewise displacement per run. The range of average run framewise displacements is reported under each group. Note, motion level 1 has fewer runs than the other motion groups to consist of runs that better match the average motion in the headpost group. *Motion Level 6 was not included in analyses due to a lack of data from censoring.

Group	Total Runs	Censored Volumes	Runs Excluded
4-Day (0.039 – 0.13 mm)	36	20.6%	5 (13.9%)
9-Day (0.015 – 0.14 mm)	74	16.2%	4 (5.41%)
13-Day (0.014 – 0.16 mm)	102	22.1%	10 (9.80%)
Headpost (0.018 – 0.027 mm)	14	0.0%	0 (0.00%)
Motion Level 1 (0.014 – 0.030 mm)	24	0.3%	0 (0.00%)
Motion Level 2 (0.031 – 0.043 mm)	38	4.2%	0 (0.00%)
Motion Level 3 (0.044 – 0.059 mm)	38	8.1%	0 (0.00%)
Motion Level 4 (0.059 – 0.071 mm)	38	14.5%	0 (0.00%)
Motion Level 5 (0.071 – 0.091 mm)	38	26.0%	0 (0.00%)
Motion Level 6* (0.091 – 0.16 mm)	36	71.5%	19 (53.8%)

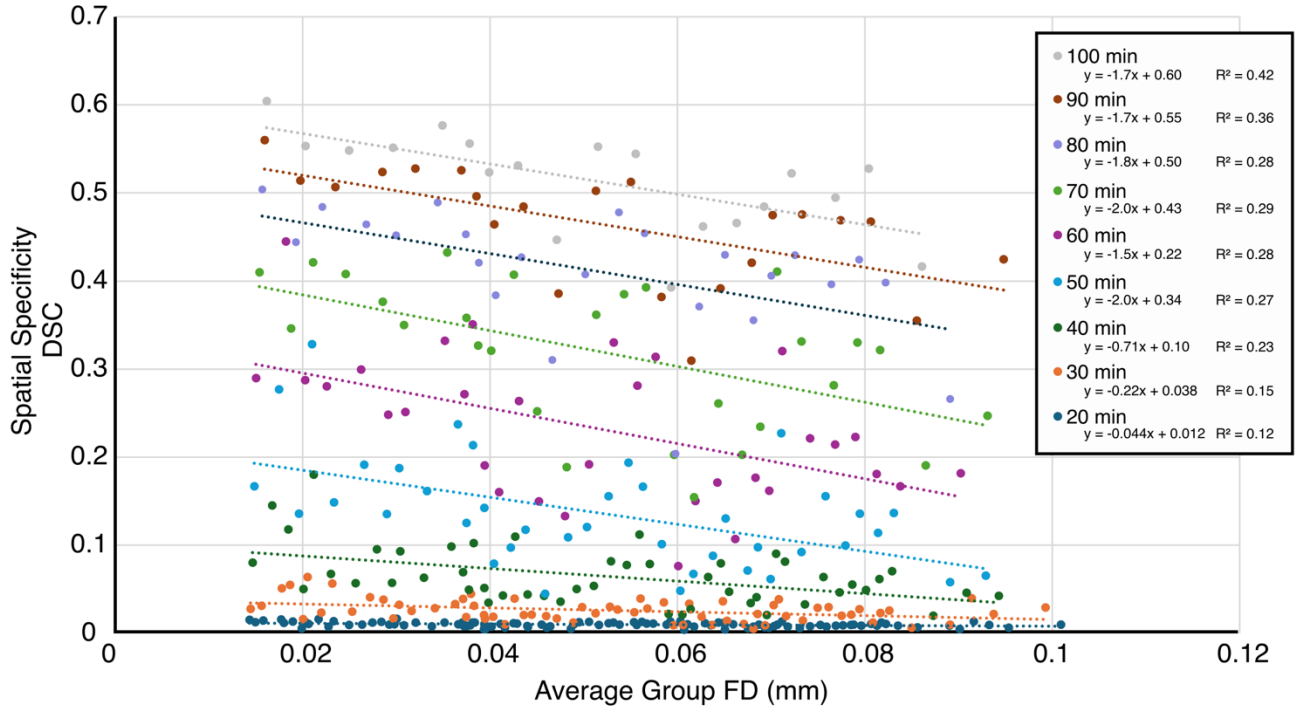

Supplementary Figure 1. Relationship between spatial specificity (Dice Similarity Coefficient, DSC) and average group framewise displacement (FD) for different group cumulative acquisition times. All functional runs were aggregated and sorted based on the average FD value. Group network spatial specificity was determined for all groups and plotted. Linear trendlines were fitted to each cumulative acquisition time groupings.

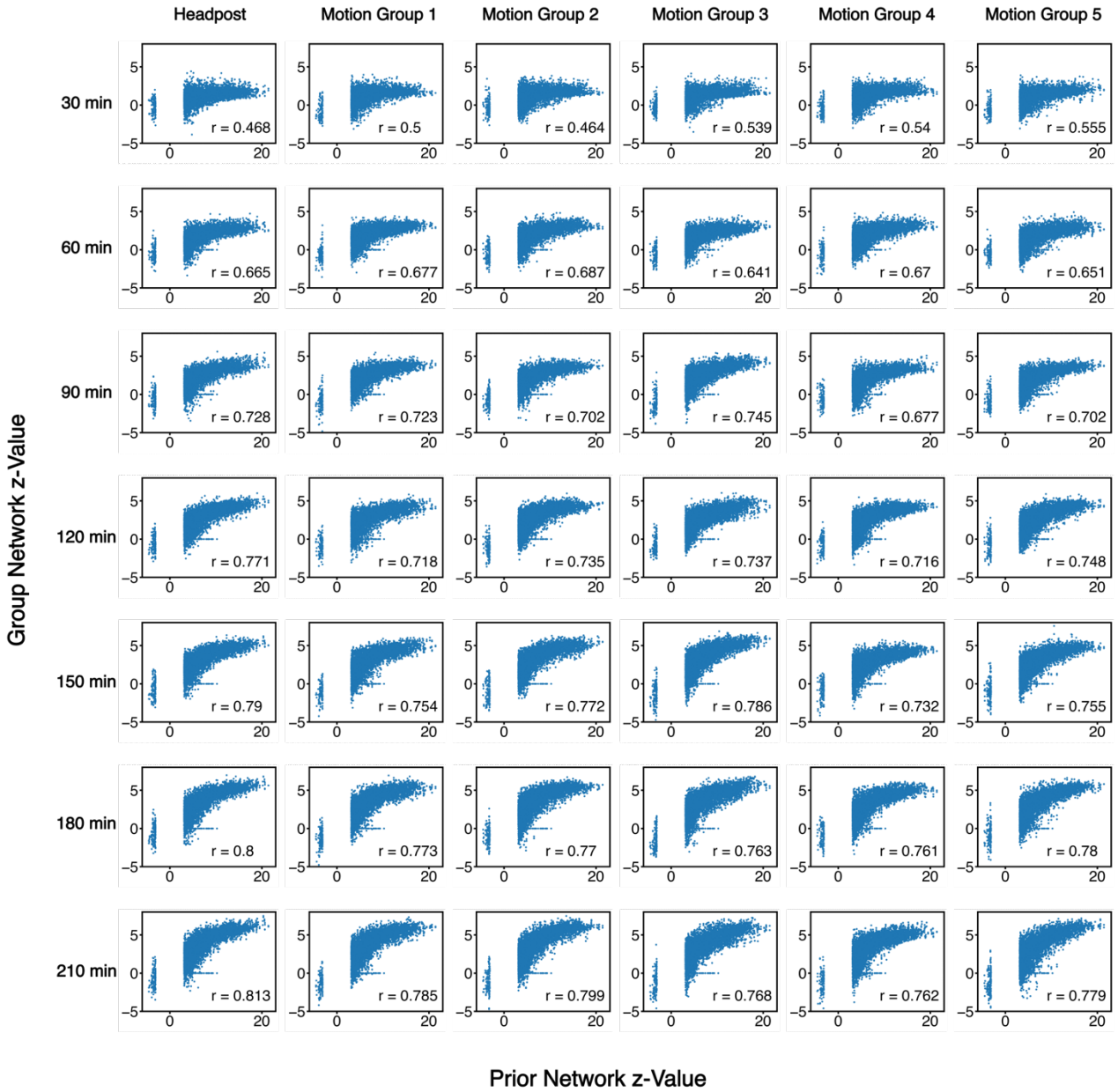

Supplementary Figure 2. Correspondence between z-values of the prior network and corresponding group networks on a voxel-wise basis for voxels in the prior network region. One sample from each group network is shown. The correlation coefficient is annotated on each plot. The gap between -3.1 and 3.1 results from masking the prior network for voxels with values >= +/-3.1 and selecting those voxels for the correlation analysis. The corresponding Pearson Correlation coefficient (r value) is annotated on each plot.

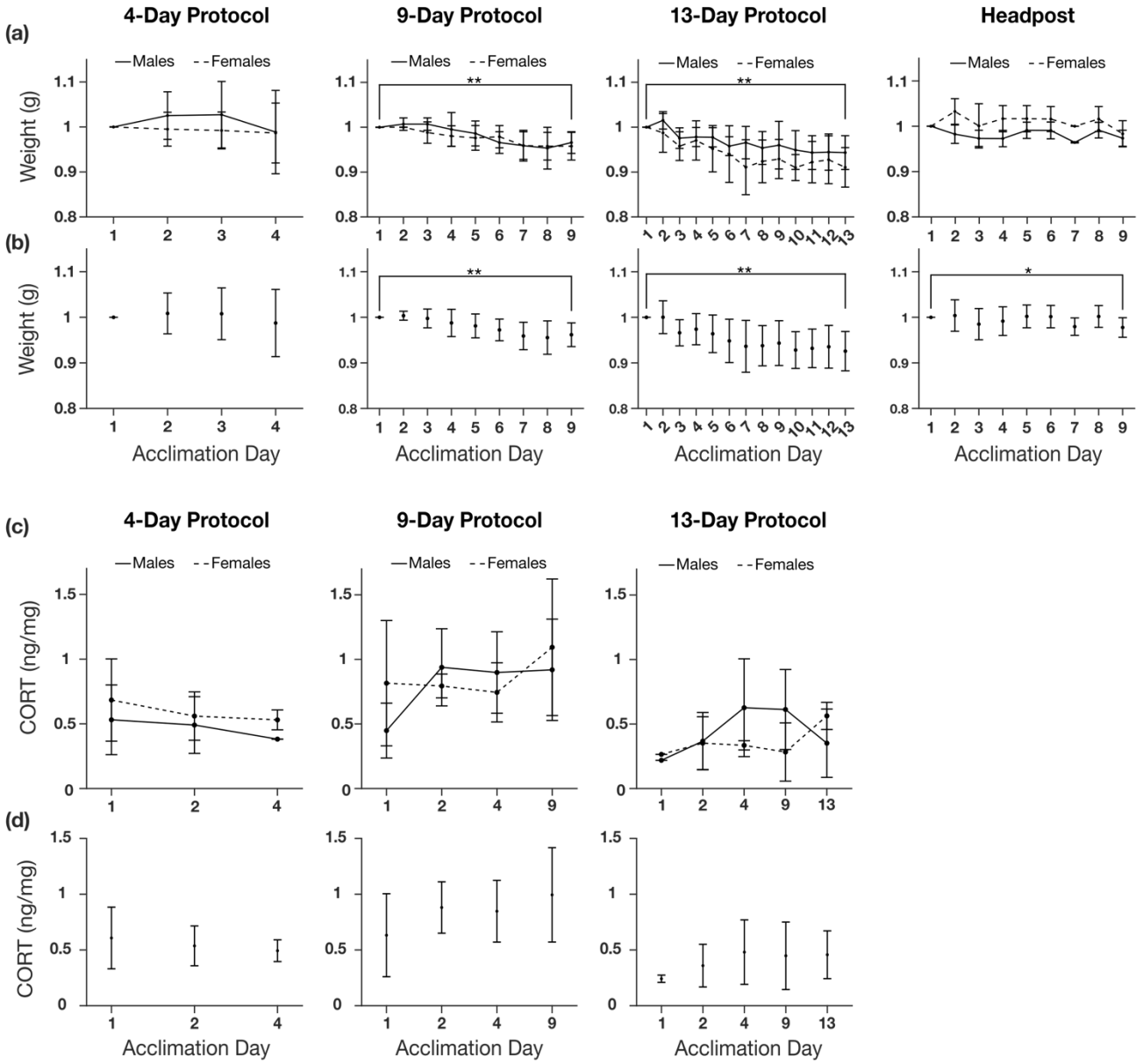

Supplementary Figure 3. Weight and fecal corticosterone (CORT) metabolite over the 3 acclimation days. (a) Weight split up by sex for the 4-day, 9-day, 13-day and headpost groups. (b) Same as (a) except both sexes aggregated. (c) CORT split up by sex for the 4-day, 9-day, and 13-day groups. (d) Same as (c) except both sexes aggregated. CORT concentrations are displayed in ng of corticosterone per mg of fecal matter. Data are displayed as group means (data points) and standard deviation (error bars).